International Journal of Heat and Mass Transfer 52 (2009) 1149–1157

Contents lists available at ScienceDirect

International Journal of Heat and Mass Transfer

journal homepage: www.elsevier.com/locate/ijhmt

Robust reduced order modeling of heat transfer in a back step flow

D. Alonso [a], A. Velazquez [a,*], J.M. Vega [b]

[a] Aerospace Propulsion and Fluid Mechanics Department, School of Aeronautics, Universidad Politécnica de Madrid, Plaza del Cardenal Cisneros 3, 28040 Madrid, Spain
[b] Applied Mathematics Department, School of Aeronautics, Universidad Politécnica de Madrid, Plaza del Cardenal Cisneros 3, 28040 Madrid, Spain

ARTICLE INFO

Article history:
Received 13 February 2008
Available online 30 October 2008

Keywords:
Singular value decomposition
Proper orthogonal decomposition
Reduced order models
Genetic algorithm
Backward facing step
Heat transfer

ABSTRACT

We present a method to obtain reduced order models to calculate steady states in thermal systems of industrial interest. The method could be regarded as an evolution of the standard proper orthogonal decomposition (POD) method, in which the reduced model is obtained through standard Galerkin projection (whose application exhibits well known difficulties) on previously obtained POD modes. Instead of relying on a Galerkin projection, we use a genetic algorithm (GA) to minimize a conveniently defined residual for the (continuity, momentum, and energy) equations and boundary conditions. The method and its practical application are illustrated on a test problem that describes heat transfer in the recirculation region downstream of a backwards facing step.

1. Introduction

A common situation in practical industrial applications related to product development is the need to perform fast calculations inside a space of design parameters. In mature, very competitive, industrial sectors like aerospace or automotive, this need is motivated by the drive to generate products having good technical performance within design cycles that are as short as feasible. Thus, time is a critical aspect of industrial competitiveness because shortening the time to market may provide a leading economic advantage during the product life cycle.

A possible way to shorten design cycles consists of replacing experiments by computational fluid dynamics (CFD) calculations. Now, if the number of parameters is not small and a fully nonlinear behavior is involved, then obtaining approximate solutions is not trivial unless a large number of numerical calculations is performed. For instance, if we consider a 2D cooling system, such as a micro-heat-exchanger, we might be interested in determining the global response of the system (through, e.g., the pressure drop from entrance to exit, the Nusselt number, and a property of the flow like the size of a recirculation bubble) in terms of the Reynolds and Prandtl numbers, the temperature difference inside the system, and a geometric parameter such as the aspect ratio. If we compute five to ten values for each parameter, the whole study requires 5^4–10^4 simulation runs. This is not to mention the case where additional geometry design parameters, such as those defining the shape of the system, are accounted for, or the case where a full 3D configuration is considered. Thus, the cost advantage associated to the use of CFD may be offset by the sheer number of numerical simulations needed. A possible way out of this dilemma is, of course, to compute a limited, well selected number of cases and to interpolate between them. However, the problem with interpolation is that accuracy degrades when either more than a few parameters are involved or the distance between available points in the parametric space is not small enough. This can be overcome somehow if interpolation is made on global modes resulting from either proper orthogonal decomposition (POD) [1] or high order singular value decomposition (HOSVD) [2] which will be done below as a part of the analysis. HOSVD [3] is an extension to tensors of classical SVD [4]; note that such extension is not straightforward and involves some subtleties [5].

An alternative method to interpolation is the use of reduced models based on approximate mathematical modeling techniques, which might be a convenient way to achieve the above mentioned practical industrial goals. These reduced models are usually obtained via a standard Galerkin projection on a set of previously calculated modes, through Proper Orthogonal Decomposition (POD). The problem is that Galerkin projection leads to reduced order models that need some kind of artificial stabilization, a difficulty that is still unsolved nowadays, especially in open flow systems and non-selfadjoint problems.

The objective of this paper is to present a method with an improved performance on industrial product development. Our method consists of three steps:

(1) A set of *snapshots* is selected with steady states of the system for representative values of the parameters, calculated using CFD. With these, POD machinery is a applied to calculate the

* Corresponding author. Fax: +34 913366351.
E-mail address: angel.velazquez@upm.es (A. Velazquez).

0017-9310/$ - see front matter © 2008 Elsevier Ltd. All rights reserved.
doi:10.1016/j.ijheatmasstransfer.2008.09.011

Nomenclature

Latin symbols

a_i^j	ith amplitude of the jth variable
BC_j	acronym for the jth imposed boundary condition
$\tilde{c}_p$	heat capacity
E_j	acronym for the jth imposed squared integral equation
$\tilde{h}$	channel height
K_i	ith mode of the thermal conductivity
m	total number of modes
M_i	ith mode of the molecular viscosity
n	number of modes taken for all variables when $n_1 = n_2 = \cdots$
n_i	number of modes taken for the ith variable
N_G	number of generations
N_I	number of individuals
Nu	Nusselt number
L_R	attachment length
p	dimensionless pressure
P_D	pressure drop
Pr	Prandtl number
$\tilde{Q}'$	heat flux
R_{ij}	covariance matrix
Re	Reynolds number
$\mathscr{R}$	residual function
$T, \tilde{T}$	dimensionless and dimensional temperature
$u, \tilde{u}$	dimensionless and dimensional horizontal velocity components
U_i	ith mode of the horizontal velocity component
$v, \tilde{v}$	dimensionless and dimensional vertical velocity components
x, y	horizontal and vertical coordinates

Greek symbols

γ_i	ith eigenvalue of the covariance matrix
∂_x, ∂_y	partial derivatives with respect to x and y
Δ	Laplacian operator
$\kappa, \tilde{\kappa}$	dimensionless and dimensional thermal conductivities
κ_1, κ_2	coefficients of dimensionless molecular viscosity polynomial
μ	dimensionless molecular viscosity
$\tilde{\mu}$	molecular viscosity
μ_1, μ_2	coefficients of dimensionless molecular viscosity polynomial
$\tilde{\rho}$	dimensional density
Ω	spatial domain

Superscripts

inlet	value at the inlet section
max	maximum value
wall	value at the wall

associated *POD modes*, and a first approximation of the solution based on *SVD plus interpolation*. The latter is to be used as initial guess in step 3 below.

(2) The flow variables (e.g., velocity components, pressure, and temperature) are expanded in terms of the POD modes. These expansions are substituted into the governing equations (e.g., continuity, Navier–Stokes, and energy equations), which are squared, integrated over the fluid domain, and added to the squares of the boundary conditions, to calculate a *residual* that should be minimized.

(3) The coefficients in the expansions above are called *amplitudes of the modes*, and are calculated as the *minimizers* of the residual, using a *genetic algorithm* (GA).

The main new ingredients in our method are in steps 2 and 3, which are more *flexible* and *robust* than their counterparts in classical POD + Galerkin methods.

Rather than formulating the method only, we both describe the method and illustrate its practical application using a *test problem*, namely *a laminar flow past a backward facing step* with temperature dependent viscosity and thermal conductivity. With these, we also intend to assess the robustness and accuracy of the method.

The use of SVD-based methods for studying thermal problems is not new. In particular, these methods have been used in inverse heat conduction problems for various purposes; namely, (a) to estimate unknown boundary conditions such as surface heat flux, surface temperature, and heat transfer coefficients [6]; (b) to control spatial and temporal instabilities through regularization [7]; and (c) to filter noisy temperature data [8]. And SVD has been also used to deal with multicomponent thermal systems, whose treatment involves a large number of differential equations [9].

Concerning the use of POD to obtain reduced order models for the Navier–Stokes equations, see a recent review by Burkardt et al. [10]. The stability of reduced models obtained via Galerkin projection on POD modes is an important issue since it has long been recognized that these methods, attractive as they are, need stabilization schemes to yield acceptable solutions. This central question is discussed in detail by Sirisup and Karniadakis [11], who point out that an erroneous state of the POD-reduced order model equations can be obtained as a large time behavior of the system even if the correct state is used to initialize the simulation. This means that the numerical solution of the reduced order model may eventually drift to a spurious state. Several stabilization methods are presented and tested in references [11,12]. See also a 'calibration method' by Galleti et al. [13], whose application requires in practice to solve an adjoint problem. An alternative 'calibrated method' has been proposed by Couplet et al. [14] that determines the free parameters of the POD system via the solution of a minimization problem. Approaches based on something more than Galerkin projection have also been proposed. In particular, Sirisup et al. [15] use de concept of projective integration [16], which consists of performing short burst of full direct numerical simulation to estimate the evolution of the flow dynamics. The use of POD based formulations to improve the efficiency of numerical simulation methods has also been proposed and studied by Tromeur-Dervout and Vassilevski [17] and Rathinam and Petzold [18]. Finally, a method that combines SVD and GA within the development of a fuzzy network has been reported by Nariman et al. [19].

The remaining of the paper is organized as follows. The method we propose is presented in Section 2, using the above mentioned test problem. The main results are given and discussed in Section 3. The paper ends with some concluding remarks, in Section 4.

2. The test problem and the reduced model

The method presented in this paper does not depend on the specific problem under consideration. However, for the sake of clarity we shall describe the method applying it to a specific test problem, which is described first. Such illustration is made with two ideas in mind:

- The application is considered only to illustrate the method. We do not intend to give a complete study of the test problem, which on the other hand includes various interesting bifurcations and instabilities. Thus, the parameter range will be selected such that only one flow topology is present.
- Our aim is to describe the method and illustrate its advantages concerning robustness and flexibility. The method can be further improved in various ways (see Section 4), but such improvement is beyond the scope of this paper.

2.1. The test problem

As a test problem, we have chosen the nonisothermal, two-dimensional flow past a backwards facing step; see Fig. 1. The flow is laminar (the Reynolds number is moderate, not larger than 500) and steady. The temperature of the incoming flow is $\widetilde{T}^{\text{inlet}} = 293$ K (with tildes denoting hereafter dimensional quantities) and all walls are adiabatic except for a portion of the bottom wall, which exhibits a length that is 10 times the step hight and is located downstream of the step (Fig. 1), where temperature is maintained at $\widetilde{T}^{\max} = 353$ K. Such temperature variation implies that if the working fluid is water, then its viscosity changes by a factor of 3 [20]. Thus, it is necessary to take into account dependence on temperature of viscosity (and of thermal conductivity, which also varies significantly). The assumption of 2D flow seems justified because previous studies on the constant viscosity case (e.g., [21,22]) have shown that 3D instabilities occur at Reynolds numbers in the range of 700–997, depending on thermal boundary conditions.

The spatial coordinates, x and y, the velocity components, u and v, and the pressure p are made dimensionless using twice the height and the velocity at the inlet section, $2\tilde{h}^{\text{inlet}}$ and $\tilde{u}^{\text{inlet}}$, respectively, and nondimensional temperature is defined as $T = (\widetilde{T} - \widetilde{T}^{\text{inlet}})/(\widetilde{T}^{\max} - \widetilde{T}^{\text{inlet}})$. The governing equations (continuity, horizontal and vertical momentum conservation, and energy conservation) are

$$\partial_x u + \partial_y v = 0, \tag{1}$$

$$u\partial_x u + v\partial_y u + \partial_x p - \frac{1}{\text{Re}}\left[\mu\Delta u + 2\partial_x\mu\partial_x u + \partial_y\mu(\partial_y u + \partial_x v)\right] = 0, \tag{2}$$

$$u\partial_x v + v\partial_y v + \partial_y p - \frac{1}{\text{Re}}\left[\mu\Delta v + 2\partial_y\mu\partial_y v + \partial_x\mu(\partial_x v + \partial_y u)\right] = 0, \tag{3}$$

$$u\partial_x T + v\partial_y T - \frac{1}{\text{RePr}}\left[\kappa\Delta T + \partial_x\kappa\partial_x T + \partial_y\kappa\partial_y T\right] = 0, \tag{4}$$

where ∂_x and ∂_y denote the partial derivatives with respect to x and y, respectively, and $\Delta = \partial^2_{xx} + \partial^2_{yy}$ stands for the Laplacian operator. The (inlet) Reynolds and Prandtl numbers are defined as $\text{Re} = 2\tilde{\rho}^{\text{inlet}}\tilde{h}^{\text{inlet}}\tilde{u}^{\text{inlet}}/\tilde{\mu}(\widetilde{T}^{\text{inlet}})$ and $\text{Pr} = \tilde{c}_p\tilde{\mu}(\widetilde{T}^{\text{inlet}})/\tilde{\kappa}(\widetilde{T}^{\text{inlet}})$, respectively, where $\tilde{\rho}$ and $\tilde{c}_p$ denote density and heat capacity, respectively. Dependence of dimensionless viscosity and thermal conductivity on temperature is assumed quadratic [20], and accounted for in nondimensional terms as

$$\mu \equiv \tilde{\mu}(\widetilde{T})/\tilde{\mu}(\widetilde{T}_{\text{inlet}}) = 1 - \mu_1\cdot T + \mu_2\cdot T^2, \tag{5}$$

$$\kappa \equiv \tilde{\kappa}(\widetilde{T})/\tilde{\kappa}(\widetilde{T}_{\text{inlet}}) = 1 + \kappa_1\cdot T - \kappa_2\cdot T^2, \tag{6}$$

where (in the temperature range we are considering in this paper, 293 K $< \tilde{T} <$ 353 K), the coefficients are

$$\mu_1 = 1.1292, \quad \mu_2 = 0.49036, \quad \kappa_1 = 0.1572, \quad \kappa_2 = 0.04704.$$

The boundary conditions are as follows. At the inlet section, $x = 0$, we impose a Poiseuille-like flow and a temperature equal to the coolant temperature, namely

$$u(y) = -24\left(y^2 - \frac{y}{2}\right), \quad v(y) = 0, \quad \partial_x p = \frac{-48}{\text{Re}}, \quad T = 0, \tag{7}$$

while at the outlet section, $x = 15$, we require that

$$\partial_x u = \partial_x v = \partial^2_{xx} p = \partial_x T = 0. \tag{8}$$

At solid walls we impose no slip and assume that the central part of the lower wall exhibits a nondimensional temperature $T = T^{\text{wall}}$, while the remaining part of the lower wall and the upper wall are thermally insulated. Namely,

$$u = v = 0, \quad T = T^{\text{wall}} \tag{9}$$

if $5 < x < 10$ and $y = 0$, and

$$u = v = 0, \quad \partial_y T = 0 \tag{10}$$

if either $0 < x < 5$ and $y = 0.5$, or $x = 5$ and $0 < y < 0.5$, or $10 < x < 15$ and $y = 0$, or $0 < x < 15$ and $y = 1$.

Note that we are giving boundary conditions for pressure at both the entrance and the exit of the domain, which in principle are not necessary because pressure is just a Lagrange multiplier in incompressible Navier–Stokes equations, which is needed to compensate for the (extra) continuity equation. But the boundary conditions for pressure are just the ones that match with parallel flow at both the entrance and exit, namely those compatible with the boundary conditions for the velocity components and the horizontal momentum equation when the additional condition $\partial_{xx} u = 0$ is imposed, as is readily seen. We give the pressure boundary conditions explicitly because these are convenient to improve precision in the analysis of next section. Also, these boundary conditions are necessary in the pseudo-compressibility approach we have followed to numerically integrate the equations (see Refs. [23,24] for details); that approach also needs a boundary condition for pressure at solid walls, which is obtained integrating (near the wall) the momentum equation in the direction perpendicular to the wall (except at the corners, where the direction that bisects the corners is considered), with one sided (into the flow domain) derivatives, and imposing no slip at the wall.

Now, in order to carry out CFD computations, we use a second order, finite point flow solver that is described elsewhere [23,24]. Steady states are calculated solving a time marching formulation

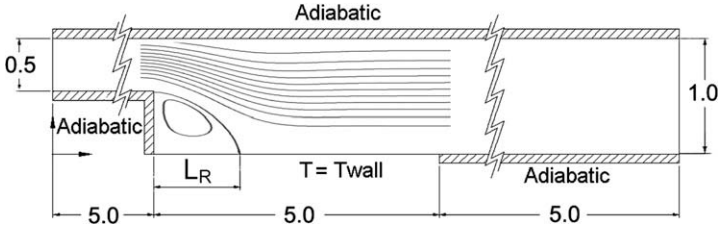

Fig. 1. Sketch of the fluid domain.

based on a pseudo-compressibility approach, as stated above. The mesh is Cartesian, with 32,051 points and a (nondimensional) distance between points of 0.02.

The simplest non-attached steady state of the system shows a unique recirculation bubble just behind the step, as sketched in Fig. 1. In isothermal conditions, such steady state can be somewhat characterized by means of the *length of the recirculation bubble* (see Fig. 1), L_R, and the *pressure drop* from entrance to exit, P_D. In non-isothermal conditions we shall also consider the *Nusselt number*, defined as

$$\mathrm{Nu} = \frac{\widetilde{Q}'}{2(\widetilde{T}^{\max,\mathrm{wall}} - \widetilde{T}^{\mathrm{inlet}})\tilde{\kappa}(T^{\mathrm{wall}})\tilde{h}^{\mathrm{inlet}}} \equiv \int_5^{10} \partial_y T(x,0)dx, \tag{11}$$

where $\widetilde{Q}'$ is the (dimensional) heat flux in the nonadiabatic part of the lower wall, and κ is the dimensional thermal conductivity. This simple steady state exists for intermediate Reynolds numbers, as $\mathrm{Re}_1 < \mathrm{Re} < \mathrm{Re}_2$, where $\mathrm{Re}_1 \sim 5$ and $\mathrm{Re}_2 \sim 600$ in isothermal conditions. The recirculation bubble disappears as Re approaches Re_1 and splits into several bubbles as Re approaches Re_2. Since the test problem is only intended to illustrate our method, we shall concentrate in the intermediate values of Re and will avoid approaching the bounds Re_1 and Re_2.

2.2. Snapshots, POD modes, and SVD plus interpolation

The snapshots must be representative of the parameter range we intend to cover, and will be selected accordingly in Section 3. Each snapshot gives the steady state of the system for a specific set of values of the parameters, which requires to give the velocity components, pressure, and temperature, namely

$$(u_k, v_k, p_k, T_k) \quad \text{for } k = 1, \ldots, N. \tag{12}$$

These snapshots allow us to obtain the POD modes, which are calculated independently for each variable (a main difference with the standard POD + Galerkin approach) using standard formulae. For instance, POD modes for the horizontal velocity are given by

$$U_j = \sum_{k=1}^{N} \alpha_j^k u_k. \tag{13}$$

The coefficients $\alpha_1^k, \ldots, \alpha_N^k$ are the eigenvectors of the positive definite, symmetric $(N \times N)$-matrix R, known as the *covariance matrix*, defined as

$$R_{ij} = \langle u_i(x,y), u_j(x,y) \rangle \tag{14}$$

in terms of the L_2-inner product

$$\langle u_i(x,y), u_j(x,y) \rangle = \int_\Omega u_i(x,y) u_j(x,y) dxdy, \tag{15}$$

where Ω stands hereafter for the following spatial domain

$$\Omega = \{(x,y) \in \mathbb{R}^2 : 5.5 < x < 10.0 < y < 1\}. \tag{16}$$

This domain has been chosen such that it (a) covers most part of the recirculation bubble and (b) avoids that corner region on the upper part of the step, where CFD calculations show largest localized errors do to a singularity in the velocity gradient (see our remarks on this point in Section 4). Note that we are not taking as Ω the whole fluid domain, as usually done in standard POD + Galerkin approaches.

Now, if the expansion (13) is truncated to $n \leqslant N$ terms, then the relative error in terms of the L_2-norm associated with (15) is bounded by

$$|\mathrm{error}| \leqslant \sqrt{\frac{\sum_{i=n+1}^{N} \gamma_i}{\sum_{i=1}^{N} \gamma_i}}, \tag{17}$$

where $\gamma_1 \geqslant \ldots \geqslant \gamma_N \geqslant 0$ are the eigenvalues of the matrix (14). This gives an a priori estimate of the number of POD modes that must be retained to obtain a fixed error. The POD modes are now used to write down the flow variables as

$$u(x,y) = \sum_{i=1}^{n_1} a_i^1 U_i(x,y), \quad v(x,y) = \sum_{i=1}^{n_2} a_i^2 V_i(x,y), \tag{18}$$

$$p(x,y) = \sum_{i=1}^{n_3} a_i^3 P_i(x,y), \quad T(x,y) = \sum_{i=1}^{n_4} a_i^4 \theta_i(x,y), \tag{19}$$

where the coefficients $a_i^1, \cdots, a_i^4$ are the *amplitudes of the modes*; these are unknowns to be determined below. Although the number of modes in each variable needs not be the same (see comment on this point in Section 4), for simplicity we assume hereafter that

$$n_1 = \cdots = n_4 = n. \tag{20}$$

Let us now calculate a *first approximation* of these amplitudes for arbitrary parameter values using *SVD + interpolation*, which requires to take into account the parameter values for which the N snapshots (12) have been calculated, namely

$$\mathrm{Re}_1, \ldots, \mathrm{Re}_N \tag{21}$$

if only one parameter (the Reynolds number) is considered, or

$$\mathrm{Re}_1, \ldots, \mathrm{Re}_{N_1}, \quad T_1^{\mathrm{wall}}, \ldots, T_{N_2}^{\mathrm{wall}}, \tag{22}$$

with $N = N_1 \times N_2$, if dependence on a second parameter (the wall temperature) is also accounted for. We intend to calculate the amplitudes of the modes in terms of these parameters, namely

$$a_i^j = a_i^j(\mathrm{Re}) \quad \text{or} \quad a_i^j = a_i^j(\mathrm{Re}, T^{\mathrm{wall}}), \tag{23}$$

which will be done in two steps: (a) at the parameter values associated with the snapshots, (21) or (22), the amplitudes of the modes, $a_i^j = a_i^j(\mathrm{Re}_k)$ or $a_i^j = a_i^j(\mathrm{Re}_k, T_l^{\mathrm{wall}})$, are calculated just projecting the snapshots (12) into the POD basis; and (b) at the remaining (intermediate) values of the parameter(s) the amplitudes of the modes (23) are calculated using cubic (spline) interpolation on the amplitudes a_i^j.

2.3. Preprocessing to calculate the residual

As anticipated above, next step consists of calculating the amplitudes of the modes (i.e., the coefficients in the expansions (18), (19)) minimizing a conveniently defined global error. This global error will be called the *residual* below, and will be obtained (in rough terms) substituting the expansions into the governing equations and boundary conditions, squaring, and integrating. In a first attempt, we set

$$\mathrm{Residual} = \sum_{l=1}^{4} \int_\Omega (E_l(x,y))^2 dxdy + \sum_{l=1}^{3} (BC_l)^2, \tag{24}$$

where the spatial domain Ω is as defined above, in (16), $E_1, \ldots, E_4$ are the left hand sides of Eqs. (1)–(4), and

$$\begin{aligned} BC_1 &= \int_{0.5}^{1} u(0,y)dy - \frac{1}{2}, \\ BC_2 &= \frac{1}{0.84 - 0.66} \int_{0.66}^{0.84} \partial_x p(0,y)dy + \frac{48}{\mathrm{Re}}, \\ BC_3 &= \int_5^{10} T(x,0)dx - 5T^{\mathrm{wall}} \end{aligned} \tag{25}$$

account for the nonhomogeneous boundary conditions in (7)–(9). Here, we are taking into account that the u-profile at the entrance ($x = 0$) is Poiseuille for both the POD modes and the solution we are approximating, and that similarly, the pressure gradient at $x = 0$ and the temperature at the nonadiabatic part of the wall are

both constant. Thus, imposing each boundary condition only requires to impose one integral condition (instead of imposing the boundary condition pointwise, as should be done in principle). Note that the contribution of the pressure boundary condition at the inlet section, BC_2, is calculated only in the subinterval $0.66 < y < 0.84$ thus avoiding two regions near the wall where localized numerical errors on the pressure gradient are present; see remark on this point in Section 4.

Now, calculating the residual (which should be done at each step of the minimizing process, see next section) requires to calculate the various integrals appearing in (24), which is fairly expensive numerically. Computational cost can be much lowered taking advantage of the fact that nonlinearity is algebraic (in fact, cubic), which allows a preprocessing that requires to calculate the integrals just once. The resulting expression of the residual would be

$$\text{Residual} = \mathscr{R}(a_1^1, \ldots, a_n^1, \ldots, a_1^4, \ldots, a_n^4), \tag{26}$$

where $\mathscr{R}$ is a positive definite, sixth order polynomial in $m = 4 \times n$ variables (the amplitudes of the modes), which exhibits $(4 \times n)^6$ (roughly) coefficients that should be calculated and stored. Now, the polynomial is sixth order because it contains the square of cubic (diffusive) terms in Eqs. (2)–(4), which are cubic because μ or κ depend quadratically on temperature. That cubic nonlinearity can be avoided modifying the procedure in two steps: (a) Eqs. (5) and (6), namely

$$\mu - 1 + \mu_1 \cdot T - \mu_2 \cdot T^2 = 0, \quad \kappa - 1 - \kappa_1 \cdot T + \kappa_2 \cdot T^2 = 0, \tag{27}$$

are kept as equations instead of substituting them into (2), (3); and (b) μ and κ are added as state variables. Step (a) requires to redefine the residual as

$$\text{Residual} = \sum_{l=1}^{6} \int_\Omega (E_l(x,y))^2 dxdy + \sum_{l=1}^{3} (BC_l)^2, \tag{28}$$

where $E_1, \ldots, E_4$ and BC_1, BC_2, BC_3 are still as in (24), and E_5 and E_6 are the left hand sides of the new equations (27). And step (b) requires to also calculate POD modes for the new variables, which should be expanded as

$$\mu(x,y) = \sum_{i=1}^{n} a_i^5 M_i(x,y), \quad \kappa(x,y) = \sum_{i=1}^{n} a_i^6 K_i(x,y). \tag{29}$$

Replacing these and (18), (19) into (28), we obtain (cf. (26))

$$\text{Residual} = \mathscr{R}(a_1^1, \ldots, a_n^1, \ldots, a_1^6, \ldots, a_n^6), \tag{30}$$

where now the function $\mathscr{R}$ is a *fourth order* polynomial in $m = 6 \times n$ variables, which requires to calculate and store $(6 \times n)^4$ coefficients, instead of the $(4 \times n)^6$ coefficients we had before. Eq. (30) can also be written as

$$\begin{aligned}\text{Residual} = {} & \mathscr{R}_0 + \mathscr{R}^i_{1\,j} a_i^j + \mathscr{R}^{i_1 i_2}_{2\,j_1 j_2} a_{i_1}^{j_1} a_{i_2}^{j_2} + \mathscr{R}^{i_1 i_2 i_3}_{3\,j_1 j_2 j_3} a_{i_1}^{j_1} a_{i_2}^{j_2} a_{i_3}^{j_3} \\ & + \mathscr{R}^{i_1 i_2 i_3 i_4}_{4\,j_1 j_2 j_3 j_4} a_{i_1}^{j_1} a_{i_2}^{j_2} a_{i_3}^{j_3} a_{i_4}^{j_4},\end{aligned} \tag{31}$$

where we are using Einstein summation convention (repeated indexes are summed over, for $i, i_1, \ldots, i_4 = 1, \ldots, n$ and $j, j_1, \ldots, j_4 = 1, \ldots, 6$). The various coefficients depend only on the parameters and are given in terms of integrals of products of the snapshots. For the sake of brevity, we omit here the expressions of the various tensors appearing in (31), which on the other hand are somewhat sparse, namely the coefficients are zero for many combinations of the indexes. For instance, $\mathscr{R}^{i_1 i_2 i_3 i_4}_{4\,j_1 j_2 j_3 j_4}$ has at most $19 \times n^4$ nonzero elements, instead of the $(6 \times n)^4$ elements that could be involved in this tensor.

2.4. The genetic algorithm

Now, we use a *genetic algorithm* (GA) to obtain the global minimum of the residual defined in Eq. (31), which depends on $m = 6 \times n$ *variables* (the amplitudes a_i^j). The algorithm uses N_I (to be selected below, in Section 3.1) *individuals*, each of whom exhibits m *chromosomes* (the amplitudes a_i^j); each chromosome in turn consists of 8 *genes*, which are the bits that codify this particular amplitude. *Fitness* of an individual is defined according to the value of the residual (31) associated to their genes. The GA allows the individuals to compete between themselves, mutate, and breed, as follows. The algorithm uses an initial number, $0.1 \times N_I$, of equal individuals with the genes obtained by SVD + interpolation, and the remaining $0.9 \times N_I$ with randomly chosen genes. At the beginning of every generation the individuals are ordered according to their fitness. The first $0.1 \times N_I$ are called *elite individuals*, which survive to the next generation no matter what the results of the following operations could be. The remaining individuals compete randomly between them, namely two randomly chosen individuals compare their fitness and the more fit survives; such competition is made $0.72 \times N_I$ times. Then, the *survivors* cross their genes in randomly chosen pairs to produce $0.9 \times N_I$ *new individuals* whose genes are chosen randomly from the genes of the parents. One out of every 1500 of the genes of each new individual suffers a further *random mutation*. The resulting new individuals plus the elite individuals form the population for the next generation. The whole process is repeated for N_G (to be selected below, in Section 3.1) generations. At the end, the individual with the smaller fitness is considered the optimal individual and its genes are assumed to codify the solution of the minimization problem.

3. Results

We organize this section into three subsections. First, we somewhat optimize the GA parameters N_I and N_G for this particular implementation. Then, we consider the isothermal problem (namely, with a wall temperature just behind the step identical to the cooling temperature) depending on just one parameter, the Reynolds number. Finally, Section 3.3 deals the nonisothermal problem depending on two parameters, namely the Reynolds number and the wall temperature.

3.1. Calibrating the genetic algorithm

Let us look for 'optimal' values of the two GA operational parameters that were kept free in Section 2.4, namely N_I and N_G. Such selection will be done empirically in the isothermal case, considering eight combinations of snapshots and modes, namely

- 3 snapshots, at Re = 25, 325, and 475, and 3 modes.
- 4 snapshots, at Re = 25, 175, 325, and 475, and 4 modes.
- 5 snapshots, at Re = 25, 150, 200, 325, and 475, and 5 modes.
- 10 snapshots, at Re = 25, 75, 125, 175, 225, 275, 325, 375, 425, and 475, and either 5 or 10 modes.
- 15 snapshots, at Re = 25, 50, 75, 125, 150, 175, 200, 225, 275, 300, 325, 350, 375, 425, 450, and 475, and either 5, 10, or 15 modes.

By *number of modes* we mean hereafter the number n of POD modes we are retaining in each flow variable, the total number of mode amplitudes being $m = 4 \times n$. As test cases to check results in GA calibration, we consider those for Re = 100, 250, and 400. The calculation has been performed for all combinations of values of the parameters that result from the values $N_I = 5000, 10,000,$ and $15,000$ and $N_G = 200, 400, 600, 800,$ and 1000.

This calibration produces the values $N_I = 5000$ and $N_G = 1000$ as 'optimal'. We have checked that it gives good results in the nonisothermal case too.

3.2. Results for the isothermal case

In the isothermal case, we intend to describe the steady state of the system for varying Reynolds number in the range $50 \leqslant \mathrm{Re} \leqslant 500$. The results below will be checked in three *test points*, for Re = 100, 325, and 450, which show the following values of the attachment length L_R and the pressure drop P_D:

- Test case #1 (Re = 100): $L_R = 1.40$, $P_D = 2.66$.
- Test case #2 (Re = 325): $L_R = 3.42$, $P_D = 0.56$.
- Test case #3 (Re = 450): $L_R = 4.24$, $P_D = 0.31$.

As a first combination of snapshots, we consider seven equispaced snapshots, namely

A: 7 snapshots, at Re = 50, 125, 200, 275, 350, 425, and 500. After checking the results for the three test points above, it turns out that the worse case is that for Re = 100; the obtained values of L_R and P_D in this case are given in the first row in Tables 1 and 2, respectively, where the SVD initial values are also indicated in parenthesis. These results indicate that retaining five modes provides reasonable results, namely within 4% in L_R and within 2% in P_D. This is not bad, since only required 7 snapshots. But a question arises on whether this result can be improved by a better selection of the snapshots. Since the results indicate that the low Reynolds number region requires a better approximation, we concentrate the snapshots in this region. Three ad hoc combinations of snapshots are considered, namely,

B: 6 snapshots, at Re = 50, 75, 150, 250, 350, and 500.

C: 7 snapshots, at Re = 50, 75, 125, 175, 250, 350, and 500.

D: 8 snapshots, at Re = 50, 75, 125, 175, 225, 300, 400, and 500.

Results for the four combinations are given in Tables 1 and 2, where we can see that combination B with five modes significantly improves the results obtained with combination *A*, namely both L_R and P_D are now approximated within 1.5%, which is in fact of the order of the error in CFD; thus enlarging the number of snapshots (combinations C and D) cannot provide better results, as can be seen in Tables 1 and 2. The main conclusions are that (i) the GA generally improves the initial SVD approximation, and (ii) if the snapshots are selected appropriately, then the number of snapshots is not much larger than the number of required modes. The latter is consistent with the fact that determining a *n*-dimensional linear manifold should only require to impose that it passes through *n* linearly independent points.

Now, combination B with five snapshots also provides a quite good approximation of the velocity and pressure fields. Errors are within 1.1% for horizontal velocity and pressure; errors for the vertical velocity are larger, of the order of 4.2% as expected noting that we are talking about relative errors and the absolute value of the vertical velocity is somewhat small. The associated streamlines and isobars for the three test cases are plotted with dashed lines in Fig. 2, where for comparison their counterparts obtained from CFD are also plotted with solid lines. Note that errors in isobars are large in some regions, but this is just a geometrical artifact of plotting contours of almost constant functions. In order to illustrate that, we plot in Fig.3 two sections (at constant x) of the pressure profiles in the regions where isobars show largest errors.

Table 1
Attachment length in the isothermal case obtained by the GA at Re = 100 for the various combinations of snapshots, A, B, C, and D, retaining 3, 4, or 5 POD modes; the initial value obtained using SVD + interpolation is indicated in parenthesis. The CFD value of the attachment length in this case is $L_R = 1.40$.

Attachment length	3 Modes	4 Modes	5 Modes
Combination A	1.50 (1.38)	1.46 (1.44)	1.46 (1.44)
Combination B	1.38 (1.40)	1.42 (1.42)	1.40 (1.38)
Combination C	1.40 (1.40)	1.42 (1.42)	1.40 (1.40)
Combination D	1.42 (1.40)	1.44 (1.42)	1.42 (1.40)

Table 2
As in Table 1 but giving the pressure drop instead of the attachment length. The CFD value is $P_D = 2.70$.

Pressure drop	3 Modes	4 Modes	5 Modes
Combination A	2.76 (3.06)	2.76 (3.06)	2.76 (3.06)
Combination B	2.74 (2.48)	2.74 (2.48)	2.67 (2.48)
Combination C	2.75 (2.60)	2.70 (2.60)	2.70 (2.60)
Combination D	2.73 (2.60)	2.70 (2.60)	2.70 (2.60)

3.3. Results for the nonisothermal case

We shall consider the parameter range $0 \leqslant \mathrm{Re} \leqslant 250$ and $0 \leqslant T^{\mathrm{wall}} \leqslant 1$. Note that (in comparison with the isothermal case) we have shortened the range in the Reynolds number. This has been done to avoid more complex (multi-recirculation bubble) flow topologies, which are more easily triggered in nonisothermal conditions. We consider five test cases, at various combinations of the Reynolds number and the wall temperature, which show the indicated values of the attachment length L_R, the pressure drop P_D, and the Nusselt number Nu, namely

- Test case #4 (Re 75, $T^{\mathrm{wall}} = 0.125$): $L_R = 1.14$, $P_D = 3.71$, Nu = 0.68.
- Test case #5 (Re 75, $T^{\mathrm{wall}} = 0.875$): $L_R = 1.26$, $P_D = 3.58$, Nu = 4.48.
- Test case #6 (Re 175, $T^{\mathrm{wall}} = 0.375$): $L_R = 2.24$, $P_D = 1.38$, Nu = 2.47.
- Test case #7 (Re 225, $T^{\mathrm{wall}} = 0.125$): $L_R = 2.64$, $P_D = 1.00$, Nu = 1.03.
- Test case #8 (Re 225, $T^{\mathrm{wall}} = 0.875$): $L_R = 2.76$, $P_D = 0.98$, Nu = 6.15.

The following combination of snapshots will be used:

E: 9 snapshots, at all combinations of Re = 50, 150, and 250, and $T^{\mathrm{wall}} = 0, 0.5$, and 1.

Now, as in the isothermal case, we have applied both SVD + interpolation and POD + GA to reconstruct the solution in the test cases #4–#8. It turns out that the largest absolute errors are obtained for the test case #4, while the largest relative errors correspond to test cases #7 and #8; the calculated values using POD + GA of the attachment length, pressure drop, and Nusselt numbers for these three points are

- Test case #4: $L_R = 1.00(1.04)$, $P_D = 3.78(4.54)$, $\mathrm{Nu} = 0.61(0.62)$,
- Test case #7: $L_R = 2.68(2.62)$, $P_D = 0.88(1.01)$, $\mathrm{Nu} = 0.87(0.88)$,
- Test case #8: $L_R = 2.78(2.76)$, $P_D = 1.03(0.98)$, $\mathrm{Nu} = 6.15(6.16)$,

where the reconstructed values using SVD + interpolation are also given in parenthesis. A comparison with the CFD values given above shows that the SVD results are generally improved significantly. Also, we can see that the results are surprisingly good, given the few number of snapshots we have used, namely only three values of the temperature and three values of the Reynolds number to cover a part of the parameter plane, in which the flow characteristics vary significantly. For illustration, we plot with dashed lines in

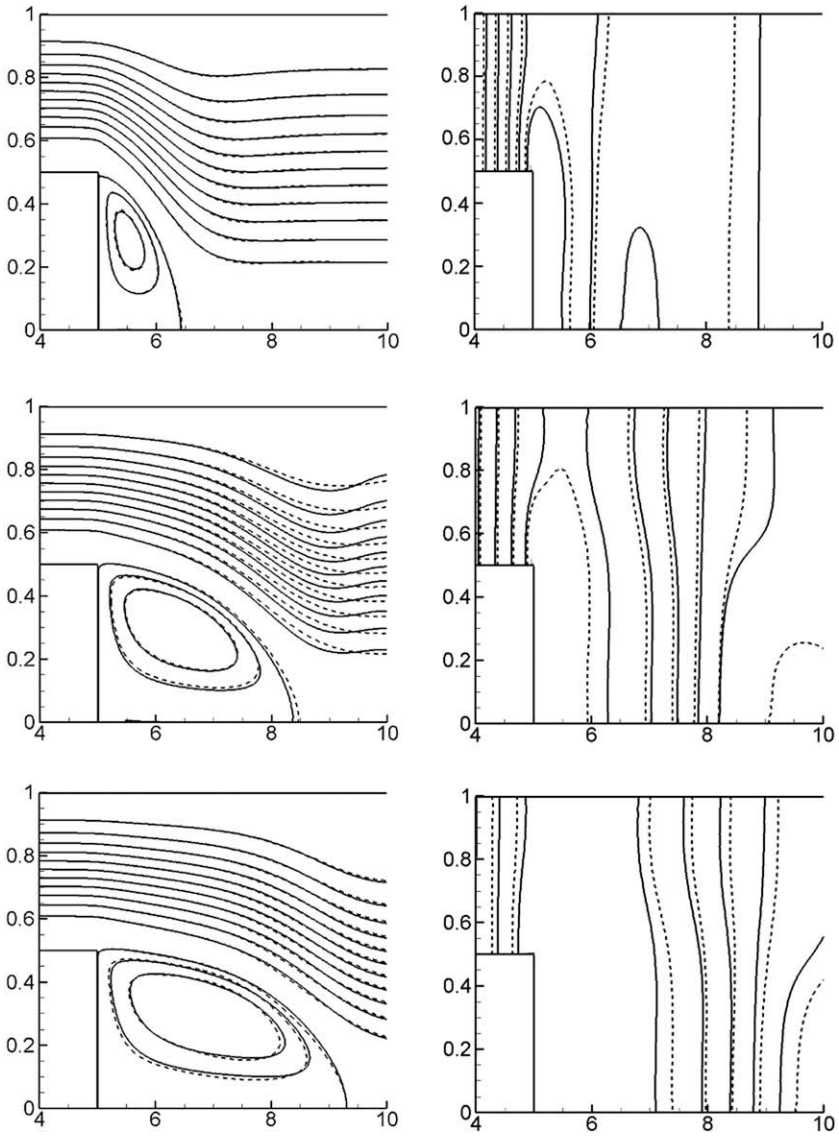

Fig. 2. Streamlines (left) and isobars (right) for the isothermal test cases #1 (up), #2 (middle), and #3 (down) as provided by CFD (—) and the method in this paper using combination B of snapshots, with 5 modes (---). For convenience, only a part of that fluid domain corresponding to $4 < x < 10$ is considered.

Fig. 4 the streamlines and isotherms for the test cases #4–#8; their counterparts obtained by CFD are also plotted with solid lines for comparison. Isobars are similar to those of the isothermal case. Again, large deviations are observed in isotherms in those regions where temperature is almost constant, but this is again an artifact of plotting contours of an almost constant function, as seen in Fig. 5.

As in the isothermal case, we could look for new combinations of snapshots that improve the (already good) result above, but it turns out that in order to do that in an appropriate way, several properties of the method (like non-equispaced selection of snapshots, or non-unit values of the weights assigned to each equation and boundary condition in the definition of the residual) should be improved, which is the object of our current research.

4. Concluding remarks

We have presented a method, based on POD and GA that provides a reduced order model to calculate the steady states of a thermal system for varying values of the parameters, at a reasonable computational cost in a robust and flexible way. The main differences with classical POD + Galerkin are that (i) instead of using a Galerkin projection, we define a residual of the governing equations, which is obtained substituting the POD expansions into the governing equations and boundary conditions, squaring, and integrating in a part of the fluid domain; and (ii) the residual is minimized using a genetic algorithm.

Some remarks concerning the method are in order:

(1) In usual POD + Galerkin approach, each POD mode is shared by all physical variables (velocity components, pressure, and temperature), which means that the amplitudes associated with these physical quantities, $a_i^1, \ldots, a_i^4$, all coincide. Our approach is more flexible. It allows (a) to impose continuity and boundary conditions (see remark 4 below), (b) to add new equations and amplitudes to reduce the computational cost, as we did in Section 2.3, and (c) to obtain better approximations using the same information, namely with the same number of snapshots, namely the number of required CFD calculations. The price is that the number of amplitudes increases, but this has generally a smaller impact in the overall computational cost.

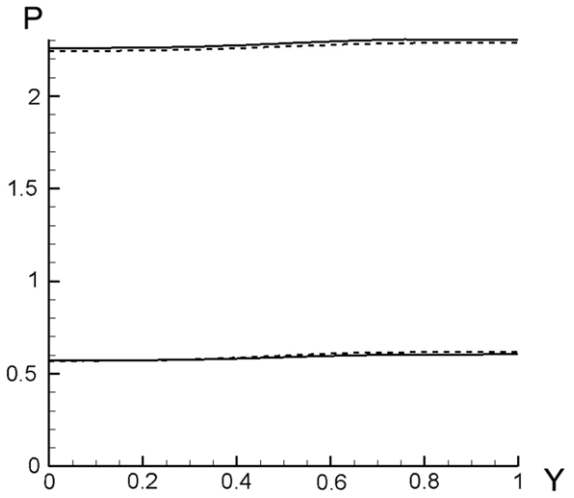

Fig. 3. Pressure profiles vs. the vertical coordinate at the section $x = 7$ for test case #1 (upper curves) and at $x = 8.5$ for test case #2 (lower curves), as provided by CFD (—) and the method in this paper using combination B of snapshots, with 5 modes (---).

(2) Our results in Section 3 indicate that the required number of snapshots can be decreased if they are chosen properly. Useful methods to choose appropriate snapshots would produce a major improvement of the method. The problem of course is that not known procedure is available for a good a priori selection of snapshots. If this were available, the method could be improved dramatically when the number of parameters is large.

(3) In connection with the previous remark, we have imposed in (20) that the number of modes in the various amplitudes all coincide. Relaxing this (which has been imposed only for the sake of clarity) is expected to decrease the required total number of modes. For instance, Eq. (27) suggests that three modes should be enough for the flow quantities μ and κ (amplitudes a_i^5 and a_i^6).

(4) The residual to be minimized (see Eq. (28) above) includes the continuity equation and the boundary conditions, which in POD + Galerkin are all assumed to hold for all snapshots (this in turn requires a somewhat artificial variable change to make all boundary conditions linear and homogeneous). But it is a fact that continuity equation is sometimes poorly

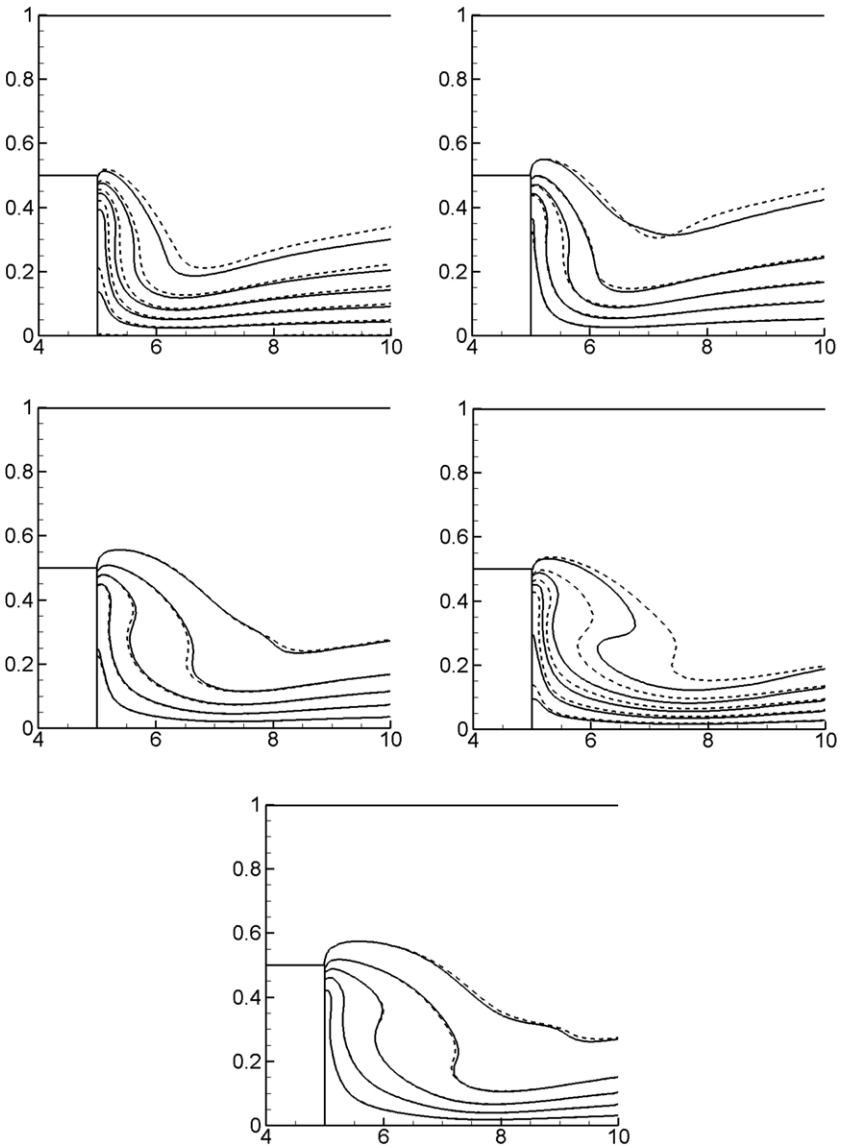

Fig. 4. Isotherms for the (nonisothermal) test cases #4 (up left), #5 (up right), #6 (middle left), #7 (middle right), and #8 (down) as provided by CFD (—) and the method in this paper (---).

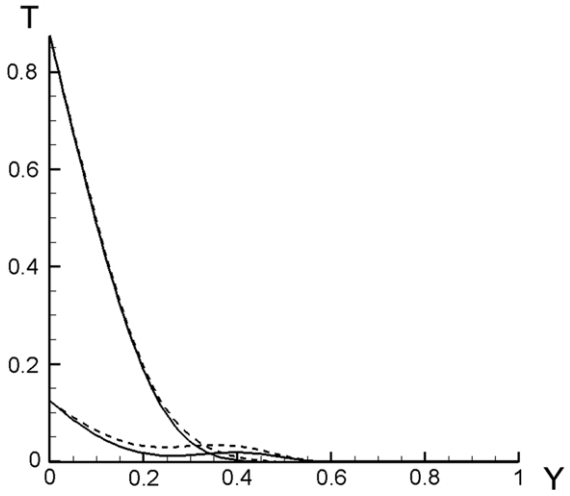

Fig. 5. Temperature profiles vs. the vertical coordinate at section $x = 6$ for test case #7 (upper curves) and at section $x = 8.5$ for test case #5 (lower curves), as provided by CFD (—) and the method in this paper using combination F of snapshots, with 5 modes (---).

satisfied by POD modes due to numerical errors. Improving continuity and homogeneous boundary conditions is nonsense in POD + Galerkin, while these are imposed in a natural way in our approach.

(5) The residual above can be defined in other ways, i.e., introducing weights (which should be calibrated for each specific application) in the equations and boundary conditions.

(6) We have only considered a part of the fluid domain, namely Ω defined in Eq. (16), to calculate the residual. This has been done because:
- On the one hand, it is by no means necessary to consider the whole fluid domain. A region containing the recirculation bubble seems to be a good selection.
- If the whole fluid domain is considered the quality of the residual may worsen due to the fact that redundant information musks the relevant information.
- If the (numerically calculated) snapshots show localized errors in some regions of the fluid domain, then these regions must be avoided when defining the working domain, as we did above when we avoided that region near the corner at the upper end of the step in the definition of Ω and a vicinity of the walls in the inlet section when defining the contribution BC_2 in Eq. (25).

(7) As in the standard POD + Galerkin approach, we could expect (in principle) spurious solutions, namely solutions of the reduced model that do not correspond to any solution of the original problem. These have not been observed in our method, which means that the global minimum of the residual seem to correspond always to a physical solution, but this does not exclude that other local minima are present that are unphysical. All these mean that our method is robust, and furthermore it does not show the kind of instabilities exhibited by Galerkin + POD.

(8) The residual has been minimized using a genetic algorithm, which is quite robust but slow. Other minimizing methods such as a steepest descend could be used, but these require a good initial guess and should be used with care.

(9) After calibration, our method produces a solution in only 2–5% of the CPU time required to obtain a CFD solution.

Summarizing, several improvements of the method are readily seen that are well beyond the scope of this paper. They are the object of our current research.

Acknowledgments

This research project has been supported by AIRBUS S.A.S under contract A8208636G, which is gratefully acknowledged. We are also indebted to Mr. Carlos Artiles, the AIRBUS Project Officer, for his help in precise identification of relevant requirements of the method in terms of daily engineering needs, and to Mr. E. Baché for checking the accuracy of some of the CFD-calculated snapshots.

References

[1] T. Bui-Thanh, Proper Orthogonal Decomposition Extensions and their Applications in Steady Aerodynamics, Master Thesis. Singapore-MIT Alliance, 2003.
[2] L.S. Lorente, J.M. Vega, A. Velazquez, Generation of aerodynamic databases using high order singular value decomposition, J. Aircraft 45 (2008) 1779–1788.
[3] L. de Lathauwer, B. de Moor, J. Vandewalle, On the best rank-one and rank-(R1, R2, RN) approximation of higher order tensors, SIAM J. Matrix Anal. Appl. 21–24 (2000) 1324–1342.
[4] G.H. Golub, G.T. Van Loan, Matrix Computations, John Hopkins University Press, 1996.
[5] V. da Silva, L.-H. Lim, Tensor rank and the ill-posedness of the best low-rank approximation problem, SIAM J. Matrix Anal. Appl. 30 (2008) 1084–1127.
[6] J.M. Gutierrez, J.A. Martin, A. Corz, A sequential algorithm of inverse heat conduction problems using singular value decomposition, Int. J. Thermal Sci. 44 (2005) 235–244.
[7] G.L. Lagier, H. Lemennier, N. Coutris, A numerical solution of the linear multidimensional unsteady inverse heat conduction problem with boundary element method and the singular value decomposition, Int. J. Thermal Sci. 43 (2004) 145–155.
[8] J.R. Shenefelt, R. Luck, R.P. Taylor, J.T. Berry, Solution to inverse heat conduction problems employing singular value decomposition and model reduction, Int. J. Heat Mass Transfer 45 (2002) 67–74.
[9] A. Yahia, E. Palomo, Thermal systems modelling via singular value decomposition: direct and modular approach, Appl. Math. Model. 23 (1999) 447–488.
[10] J. Burkardt, M. Gunzburger, H.C. Lee, POD and CVT based reduced order modelling of Navier–Stokes flows, Comput. Methods Appl. Mech. Eng. 196 (2006) 337–355.
[11] S. Sirisup, G.E. Karniadakis, Stability and accuracy of periodic flow solutions obtained by POD-penalty method, Physica D 202 (2005) 218–237.
[12] S. Sirisup, G.E. Karniadakis, A spectral viscosity method for correcting the long term behaviour of POD models, J. Comput. Phys. 194 (2004) 92–116.
[13] B. Galletti, C.H. Bruneau, C. Zannetti, A. Iollo, Low-order modelling of laminar flow regimes past a confined square cylinder, J. Fluid Mech. 503 (2004) 161–170.
[14] M. Couplet, C. Basdevant, P. Sagaut, Calibrated reduced-order POD-Galerkin system for fluid flow modelling, J. Comput. Phys. 207 (2003) 192–220.
[15] S. Sirisup, G.E. Karniadakis, D. Xiu, I.G. Kevrekidis, Equation free/Galerkin free POD assisted computation of incompressible flows, J. Comput. Phys. 207 (2005) 568–587.
[16] R. Rico-Martinez, C.W. Gear, I.G. Kevrekidis, Coarse projective kMC integration: forward/reverse initial and boundary value problems, J. Comput. Phys. 196 (2004) 474–489.
[17] D. Tromeur-Dervout, Y. Vassilevski, Choice of initial guess in iterative solution of series of systems arising in fluid flow simulations, J. Comput. Phys. 219 (2006) 210–227.
[18] M. Rathinam, L. Petzold, Dynamic iteration using reduced order models: a method for simulation of large scale modular systems, SIAM J. Numer. Anal. 40 (2002) 1446–1474.
[19] N. Nariman-Zadeh, A. Darvizeh, M.H. Dadfarmi, Design of ANFIS network using hybrid genetic and SVD methods for the modelling of explosive cutting process, J. Mater. Process. Technol. 155–156 (2004) 1415–1421.
[20] F.P. Incropera, D.P. DeWitt, Introduction to Heat Transfer, John Wiley & Sons, 1996. Table A-6, p. 764.
[21] L. Kaiktsis, G.E. Karniadakis, S.A. Orszag, Onset of three dimensionality, equilibria and early transition in flow over a backward facing step, J. Fluid Mech. 231 (1991) 501–558.
[22] D. Barkley, M.G.M. Gomes, R. Henderson, J. Fluid Mech. 473 (2002) 167–190.
[23] B. Mendez, A. Velazquez, Finite point solver for the simulation of a 2-D laminar incompressible unsteady flows, Comput. Methods Appl. Mech. Eng. 193 (2004) 825–848.
[24] A. Velazquez, J.R. Arias, B. Mendez, Laminar heat transfer enhancement downstream of a backward facing step by using a pulsating flow, Int. J. Heat Mass Transfer 51 (2008) 2075–2089.